Structure, Vol. 11, 1251–1263, October, 2003, ©2003 Elsevier Science Ltd. All rights reserved. DOI 10.1016/j.str.2003.09.001

The Crystal Structure of Plant Sulfite Oxidase Provides Insights into Sulfite Oxidation in Plants and Animals

Nils Schrader,[1,2] Katrin Fischer,[1] Karsten Theis,[1] Ralf R. Mendel,[2] Günter Schwarz,[2,*] and Caroline Kisker[1,*]

[1]Department of Pharmacological Sciences
Center for Structural Biology
State University of New York at Stony Brook
Stony Brook, New York 11794

[2]Department of Plant Biology
Technical University Braunschweig
D-38023 Braunschweig
Germany

Summary

The molybdenum cofactor (Moco) containing sulfite oxidase (SO) from *Arabidopsis thaliana* has recently been identified and biochemically characterized. The enzyme is found in peroxisomes and believed to detoxify excess sulfite that is produced during sulfur assimilation, or due to air pollution. Plant SO (PSO) is homodimeric and homologous to animal SO, but contains only a single Moco domain without an additional redox center. Here, we present the first crystal structure of a plant Moco enzyme, the apo-state of *Arabidopsis* SO at 2.6 Å resolution. The overall fold and coordination of the Moco are similar to chicken SO (CSO). Comparisons of conserved surface residues and the charge distribution in PSO and CSO reveal major differences near the entrance to both active sites reflecting different electron acceptors. Arg374 has been identified as an important substrate binding residue due to its conformational change when compared to the sulfate bound structure of CSO.

Introduction

Nitrate reductase (NR) and sulfite oxidase (SO) belong to the class of molybdenum cofactor (Moco) containing enzymes that usually catalyze two-electron redox reactions in the global C, N, and S cycles (Hille, 1996). In eukaryotes, these enzymes are important for such diverse metabolic processes as nitrate assimilation, abscisic acid biosynthesis, and purine catabolism in plants (Mendel and Schwarz, 1999) as well as sulfur detoxification and purine catabolism in mammals (Kisker et al., 1997b). SO catalyzes the overall reaction $SO_3^{2-} + H_2O \rightarrow SO_4^{2-} + 2H^+$ and $2e^-$. In all eukaryotic Mo enzymes a mononuclear Mo atom is coordinated by two sulfur atoms of a pterin derivative referred to as molybdopterin, which together form Moco (Rajagopalan and Johnson, 1992).

The existence of SO in plants has been shown only recently by the identification of a cDNA from *Arabidopsis thaliana* encoding a functional SO (Eilers et al., 2001). Immunologically crossreacting proteins of similar size were found in a wide range of plant species belonging to herbaceous and woody plants and homologous expressed sequences are available in databases. PSO has unique properties that are different from animal SOs. While animal SOs contain a Moco and a heme domain (Cohen et al., 1972), PSO lacks the heme domain (Eilers et al., 2001) (Figure 1A). Thus, among eukaryotes, PSO is the simplest Moco enzyme possessing only one redox center. Unlike animal SOs that are localized to the mitochondria (Cohen et al., 1972), PSO is a peroxisomal enzyme (Eilers et al., 2001). In animals, SO catalyzes the terminal step in the oxidative degradation of cysteine, methionine, and membrane components such as sulfatides; sulfite is oxidized to sulfate and is excreted in the urine (Johnson and Rajagopalan, 1979). Plants, however, are autotrophs that have to assimilate sulfate. During primary sulfur assimilation in chloroplasts, sulfate is converted via sulfite to organic sulfide that is essential for cysteine biosynthesis (Leustek and Saito, 1999). The important role of PSO is seen in the detoxification of excess sulfite that occurs when plants are subjected to SO_2 gas ("acid rain" as reviewed in Heber and Hüve, 1998), or when sulfur-containing compounds are degraded. The compartmentalization of sulfur assimilation and sulfite oxidation in different organelles allows plants to coregulate these opposing metabolic demands.

The crystal structure of chicken SO (CSO) was the first atomic structure (Kisker et al., 1997a) of a eukaryotic Mo enzyme. This structure has medical implications because deficiencies of this enzyme in humans lead to major neurological abnormalities and early death (Shih et al., 1977). In animals, SO is predominantly found in the liver (Cohen et al., 1972) where electrons derived from sulfite are transferred to cytochrome *c*, the physiological electron acceptor. Like all eukaryotic Moco enzymes, SO forms a dimer with a molecular mass of approximately 100 kDa and can be divided into two functional domains as observed by tryptic cleavage (Johnson and Rajagopalan, 1977). The C-terminal domain binds Moco and mediates dimer formation (Johnson and Rajagopalan, 1977), and the crystal structure revealed that these activities reside in two separate domains (Kisker et al., 1997a) (Figure 1A). The N-terminal part of animal SO constitutes the cytochrome b_5 domain that noncovalently binds the second cofactor, a heme (Figure 1A).

In the CSO structure the cytochrome b_5 domain is clearly separated from the Mo domain by a mobile and solvent exposed linker yielding a distance of 32 Å from the Mo atom to the heme Fe. This structural feature suggests either a very efficient electron transfer over this long distance, or a different position of the cytochrome b_5 domain during the electron transfer reaction enabling a closer approach between both metals (Pacheco et al., 1999). Recent studies of chicken SO revealed a strong dependency of the intramolecular electron transfer rate on solvent viscosity, thus suggesting a movement of the cytochrome b_5 domain during catalysis

*Correspondence: kisker@pharm.sunysb.edu (C.K.), g.schwarz@tu-bs.de (G.S.)

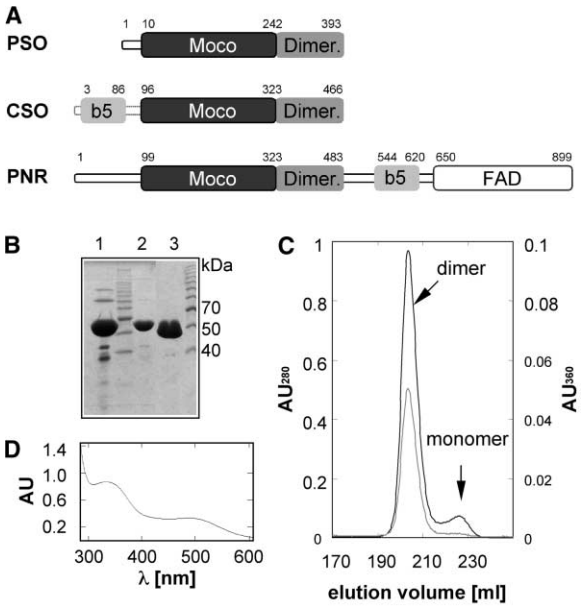

Figure 1. PSO Purification and Primary Structure Analysis

(A) Overall domain structures of PSO, CSO, and NR. Corresponding domains are indicated by the same shade of gray and the boundaries of each domain are indicated by the first and last residue number, respectively. Dimer., the dimerization domain; Moco, the Moco domain; b5, the cytochrome b_5 domain.

(B) SDS-PAGE of PSO samples after Ni-NTA affinity (lane 1), anion exchange (lane 2), and size exclusion chromatography (lane 3).

(C) Size exclusion chromatography of PSO. Absorption was detected at 280 nm (black line) and 360 nm (gray line). The peaks corresponding to dimeric and monomeric PSO are indicated.

(D) UV-VIS absorption spectrum (290–610 nm) of purified PSO (35 mg/ml) recorded in 10 mM Tris/HCl and 200 mM NaCl (pH 8.0). Absorption maxima at 360 and 480 nm are due to enedithiolate-to-molybdenum and cysteine-to-molybdenum charge transfer bonds, respectively, as assigned by resonance Raman experiments for wild-type and the C207S mutant of tryptically cleaved human sulfite oxidase yielding the Mo-domain (Garton et al., 1997).

(Feng et al., 2002). SO has been extensively studied by EPR (Astashkin et al., 2002; Codd et al., 2002; Raitsimring et al., 1998) and resonance Raman spectroscopy (Garton et al., 1997), as well as rapid kinetic methods (Brody and Hille, 1999), and a detailed model for the reaction mechanism has been published (Hille, 1996, 2002; Kisker et al., 1997b; McMaster and Enemark, 1998). The biochemical properties of PSO have been analyzed, and taking the missing heme-containing domain into account, UV-visible spectra and EPR spectra, as well as K_M values, were comparable to the vertebrate enzymes (Eilers et al., 2001).

Here we present the crystal structure of *Arabidopsis* SO at 2.6 Å resolution, the first structure of a plant Moco enzyme. The overall fold and the coordination of the cofactor are similar to the Mo domain of CSO, but larger differences are seen in the arrangement of the monomers within the SO dimers. Comparisons of conserved surface residues and charge distributions in PSO and CSO revealed major differences near the entrance to both active sites. The different levels of sequence conservation in plant and animal SOs strengthen the proposed rearrangement of the cytochrome b_5 domain in CSO and underscore the different terminal electron acceptors. Arg374 has been identified as an important residue for substrate binding due to its conformational change in the PSO apo-structure compared to the sulfate bound structure of CSO. Given the high level of sequence conservation among the Moco domains of PSO, CSO, and NR, the crystal structure suggests a similar fold for the Moco domain of NR, but highlights important differences in substrate binding.

Results and Discussion

Expression and Crystallization of PSO

PSO was purified by Ni-NTA, anion exchange, and size exclusion chromatography, resulting in a protein preparation of more than 98% homogeneity (Figure 1B). The elution profile of the size exclusion chromatography showed two peaks corresponding to monomeric and dimeric PSO (Figure 1C). Peak area integration (data not shown) revealed a roughly 20-fold excess of the dimer over the monomer. When PSO was characterized initially (Eilers et al., 2001) it was found to be predominantly monomeric, but activity was seen for both forms. Since we have observed variations in the dimer-monomer ratio among different protein batches, this finding might be due to slight changes in the purification protocol. The saturation of the protein with Moco, as followed by the absorption at 360 nm, which corresponds to the enedithiolate-to-molybdenum charge transfer bond (Figure 1D), was always higher in the dimer fraction, suggesting a tighter binding of Moco in the dimer. Therefore all subsequent work was performed with the dimeric protein.

Structure Determination

The crystal structure of *Arabidopsis* PSO was determined by molecular replacement using CSO (PDB entry 1SOX) as a search model. The resulting model has been refined to an R-factor of 23.5% (R_{free} = 26.6%) at 2.6 Å resolution (Table 1). The final model consists of residues 2 to 389 for all six monomers, one Moco, two Cs ions, and one glycerol molecule per monomer and 595 water molecules in the asymmetric unit. The Cs ions are derived from the crystallization buffer. The first and the last four residues of PSO as well as the His_6-tag are disordered in all molecules. The last three C-terminal residues, Ser, Asn, and Leu, encode a putative peroxisomal import motif (Eilers et al., 2001) and are apparently unstructured in the absence of their binding partner (Figure 2). The structure has good stereochemistry (Table 1) with 99.1% of the residues in the most favored and additionally allowed regions and no residues in disallowed regions of the Ramachandran plot as defined by PROCHECK (Laskowski et al., 1993). The overall quality of the electron density map is good and except for both termini, no disordered regions in the protein are detectable. The Moco is well defined in the $2F_o$-F_c map (Figure 3D), suggesting that the protein in the crystal is fully

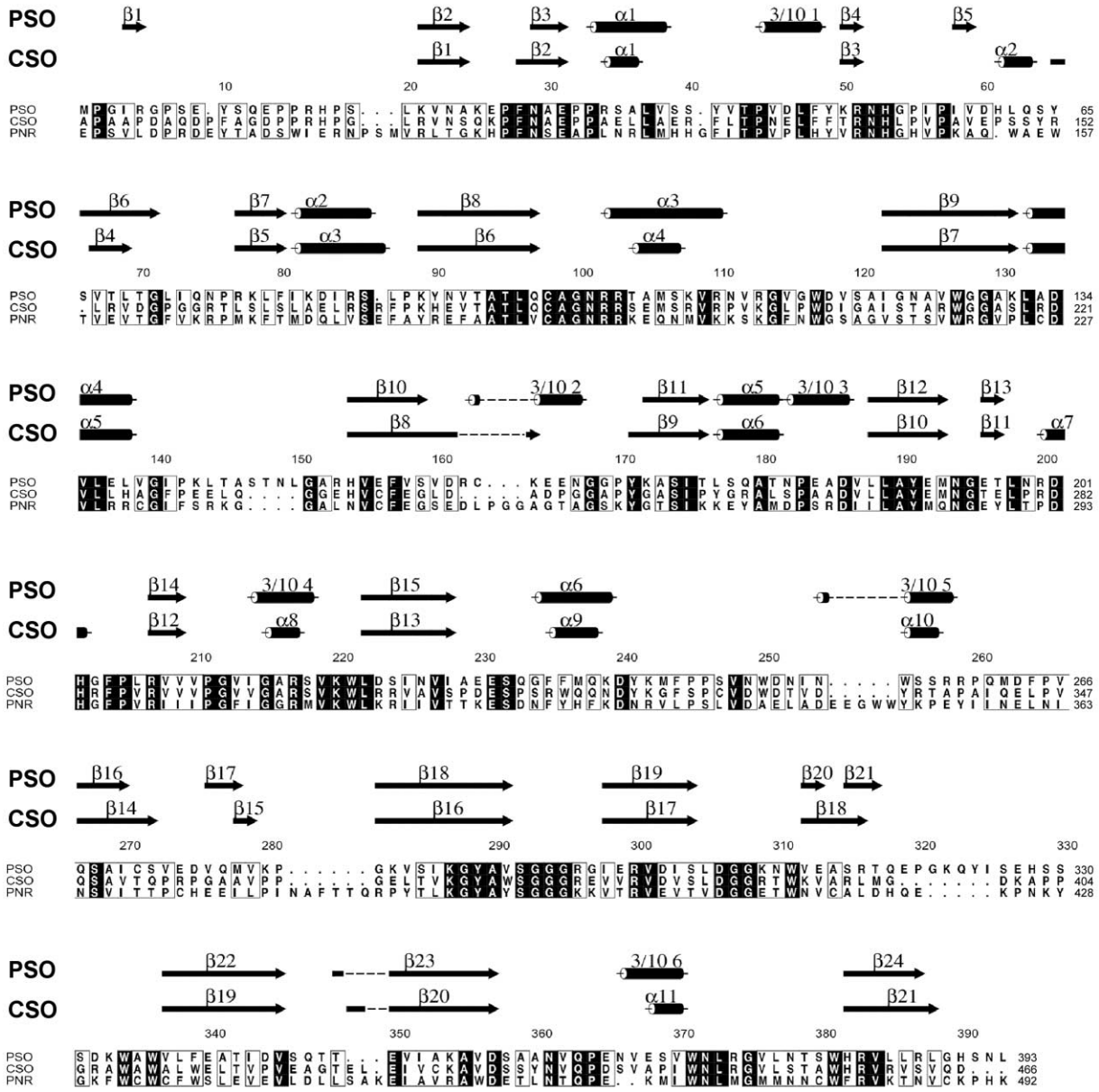

Figure 2. Primary and Secondary Structure Comparisons of PSO, CSO, and NR

Sequence alignment of PSO, CSO, and NR and comparison with the secondary structure elements of PSO and CSO. Strictly conserved and type conserved residues are highlighted in black and enclosed in a box, respectively. Secondary structure elements for PSO and CSO are shown above the alignment with arrows for β strands and cylinders for α- and 3_{10}- helices. The alignment was generated with ClustalW (Thompson et al., 1994) and ALSCRIPT (Barton, 1993). Secondary structure elements were determined with PROMOTIF (Hutchinson and Thornton, 1996). Residue numbering is based on the primary sequence of PSO. The first and last residues shown for CSO are A87 and D466 and for NR E89 and K492.

saturated with the cofactor. Two *cis*-peptides are present in PSO (Glu26-Pro27 and Phe204-Pro205), which are also found in CSO (Lys113-Pro114, Phe285-Pro286). However, one additional *cis*-peptide in CSO (Gln353-Pro354) is not present in PSO due to a lack of sequence conservation. During refinement the following two exchanges to the initially deposited PSO sequence (GenBank AF200972) have been identified: Ser206 was changed to Leu and His251 to Asp as also observed in another recent database entry (GenBank AY133863). In each case the shape of the electron density maps confirmed the altered side chain.

Fold of the Monomer

PSO is a slightly elongated molecule with an accessible surface area of about 16,160 Å^2. The fold of the PSO

Table 1. Data Collection and Refinement Statistics

Dataset	PSO
Data Collection	
Wavelength (Å)	0.90
Space group	C222
Unit cell dimensions	
—a, b, c (Å)	222.9, 351.3, 158.3
Resolution limits (Å)	30-2.6
Completeness	0.995 (0.995)
R_{sym}	0.11 (0.73)
$\langle I\rangle/\langle\sigma I\rangle$	21.6 (2.0)
Refinement Statistics	
Number of observed reflections	1,177,360
Number of unique reflections	199,819
Number of protein/cofactor atoms	36,424
Number of waters	595
R_{cryst} (R_{free})	0.235 (0.266)
Deviations from ideal values in	
—Bond length (Å)	0.034
—Bond angle distances (°)	2.614
—Torsion angles (°)	7.408
—Chiral-center restraints (Å^3)	0.177
—Plane restraints (Å)	0.013
—VDW repulsions (Å)	0.303
—Potential H-bonds (Å)	0.198
Ramachandran Statistics	88.4/10.7/0.9/0

$R_{sym} = \Sigma_{hkl}\Sigma_i|I_i - \langle I\rangle|\Sigma_{hkl}\Sigma_i\langle I\rangle$ where I_i is the ith measurement and $\langle I\rangle$ is the weighted mean of all measurements of I. $\langle I\rangle/\langle\sigma I\rangle$ indicates the average of the intensity divided by its average standard deviation. Numbers in parentheses refer to the highest resolution data shell. $R_{cryst} = \Sigma||F_o| - |F_c||/\Sigma|F_o|$ where F_o and F_c are the observed and calculated structure factor amplitudes. R_{free} same as R_{cryst} for 5% of the data randomly omitted from the refinement. Ramachandran statistics indicate the fraction of residues in the most favored, additionally allowed, generously allowed, and disallowed regions of the Ramachandran diagram, as defined by PROCHECK.

monomer can be described as a mixed $\alpha+\beta$ structure that is clearly divided into two domains (Figures 1A and 3A). The N-terminal Moco domain (residues 2 to 242) consists of 15 β strands, arranged in three antiparallel and one mixed β sheet, six α helices, and four 3_{10}-helices. The Moco is deeply buried in the center of the domain where it is surrounded by three β sheets (Figures 3A and 3C). An N-terminal antiparallel three-stranded sheet (β2–β4) leads into a five-stranded mixed β sheet (β6, β7, β10, β11, β15) on the opposite side of the domain. This sheet itself is surrounded by seven short helices (α2-α6; 3_{10}-2-3_{10}-4 helices) and is followed by a four-stranded predominately antiparallel β sheet (β8, β9, β12, β14) (Figure 3C). The central motif of this sheet comprises the two longest β strands of the domain (β8, β9), which form a β-hairpin near the interface with the C-terminal dimerization domain. Prior to the N-terminal 3-stranded β sheet, β1 and β5 form a short β-hairpin. An additional hydrophobic and polar interaction with the C-terminal domain is mediated by α3, which is located in the loop region of the aforementioned β-hairpin between residues 97 and 122.

The C-terminal dimerization domain (residues 243 to 389) is dominated mainly by two elongated β sheets containing a Greek key motif. β16, β18, β21, and β22 form the first strictly antiparallel sheet, whereas the second β sheet is predominantly antiparallel and contains strands β17, β19, β20, β23, and β24. One short helix (3_{10}-6) is located in an extended loop at the surface of the domain between β23 and β24. The overall topology of the domain is similar to the C2 subtype of the immunoglobulin superfamily as described for the corresponding domain of CSO (Kisker et al., 1997a). The last ordered residue of the dimerization domain is His389, located on the surface at a significant distance from the core of the domain. The last three residues of the native C terminus, Ser, Asn, and Leu (391-393), which presumably represent a peroxisomal import signal, are disordered. The structure indicates that this sequence is solvent accessible and does not contain a predefined structure, a feature that might be important for efficient recognition by the peroxisomal import machinery.

In the crystal structure of PSO two Cs ions derived from the crystallization buffer are bound to surface residues of each monomer. The first one is close to Ser66, Val67, and Thr68 with distances of 2.4 Å to the carbonyl oxygen of Ser66 and 3.2 Å to Oγ1 of Thr68, respectively. The corresponding residues in CSO, Arg152, Leu153, and Arg154 (Figure 2) form a positive surface potential that probably prohibits binding of cations. The second Cs ion is bound by a stretch of three serine residues (Ser329, Ser330, and Ser331) and Asp332 with Cs-ligand distances of approximately 3.3 Å (to Ser329 O, Ser330 O, and Asp332 Oδ1). Asp332 is strictly conserved in plants but varies in animal SOs. The conservation of Asp332 might indicate that this cation binding site is a unique feature of PSOs. The residues forming the second Cs binding site are located at the C-terminal end of an extended surface loop, which is also present in CSO, but adopts a completely different fold (see below).

Fold of the Dimer

As previously described for sulfite oxidases from other organisms (Johnson and Rajagopalan, 1977; Kappler et al., 2000; Kisker et al., 1997a), but in contrast to earlier studies of the plant enzyme (Eilers et al., 2001), the crystal structure of PSO clearly shows that the plant enzyme also forms a homodimer (Figures 3A and 3B). The overall dimensions of the dimer are $69 \times 59 \times 48$ Å^3. The two subunits are related by a noncrystallographic 2-fold axis and have identical structures (average rms deviation of 0.13 Å for all 388 residues of each monomer). The dimer interface is mainly composed of the dimerization domain that interacts with its counterpart, but the two Moco domains interact with each other as well. 1690 Å^2 of surface area per monomer are covered upon dimerization, corresponding to 10% of the monomer surface area. In general, the nature of the interface between the two subunits is mixed, with 43% of the residues involved in dimerization being polar and 57% hydrophobic. Within the interface 20 direct intersubunit hydrogen bonds stabilize the dimer. The number of hydrogen bonds is higher than the generally found ratio of one hydrogen bond per 200 Å^2 of buried surface (Janin et al., 1988) that would predict a total of 16 hydrogen bonds for the PSO dimer. All 20 hydrogen bonds are observed in all three dimers of the asymmetric unit, with an additional hydrogen bond between Arg153 Nη1 and Ser329 Oγ present in one dimer.

In addition to the interactions between the two

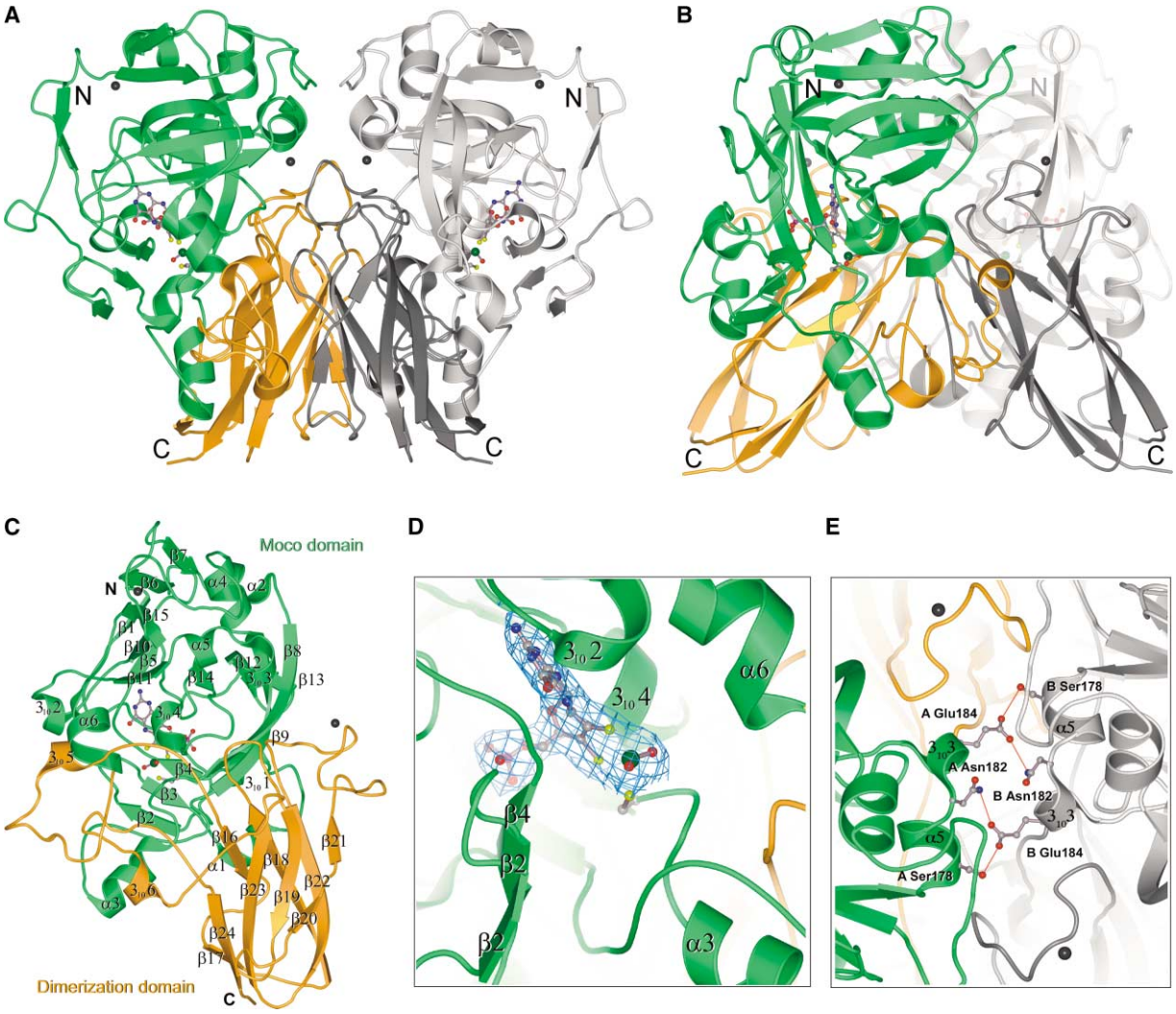

Figure 3. Overall Structure of PSO

(A) Ribbon representation of the PSO dimer viewed perpendicular to the noncrystallographic 2-fold axis. The two domains of one monomer are color coded in green (Moco domain) and orange (dimerization domain). The second monomer is shown in shades of gray, the Moco in ball-and-stick representation, β strands as curved arrows, and α- and 3_{10}-helices as helical ribbons. The bonds between Mo and all three sulfur ligands (dithiolene and Cys98) are not shown. The two Cs atoms per monomer are indicated as dark gray spheres.

(B) View of the dimer rotated by 90° compared to (A) along the rotation axis of the monomers.

(C) Ribbon representation of the monomer with secondary structure elements labeled.

(D) Close up view of the Moco with its SIGMAA weighted $2F_o$-F_c electron density map contoured at 1.0 σ. Moco and Cys98 are shown in ball-and-stick representation.

(E) Monomer-monomer interactions between the Moco domains mediated by helices α5 and 3_{10}-3. Hydrogen bonds are indicated by red lines. Figures 3, 5, and 7A were generated with MOLSCRIPT (Kraulis, 1991) and rendered with POVRAY 3.1 (http://www.povray.org).

C-terminal dimerization domains three side chains from the Moco domain form four direct hydrogen bonds to the other monomer: Ser178 Oγ binds to Glu184 Oϵ2 and Asn182 Nδ2 binds to Glu184 Oϵ1 (Figure 3E). Interestingly, these residues are all located on two short and adjacent helices, α5 and 3_{10}-3, respectively, and interact with the corresponding residues of the other monomer. Therefore, this helical region of the Moco domain is a structural element that significantly contributes to dimerization. No conserved water molecules were observed in the interfaces of the three dimers present in the asymmetric unit. The two Moco containing redox active sites of the dimer are 37.5 Å (Mo-Mo distance) apart and both catalytic units appear independent as originally proposed for the CSO structure (Kisker et al., 1997a).

The Moco Domain

As in all structurally characterized Mo enzymes (Dias et al., 1999; Dobbek et al., 1999; Enroth et al., 2000; Kisker et al., 1997a; Romao et al., 1995; Schindelin et al., 1996; Truglio et al., 2002), the Moco found in the crystal structure of PSO consists of a tricyclic pterin moiety formed by the fusion of the pyran ring to a pyrazine ring of

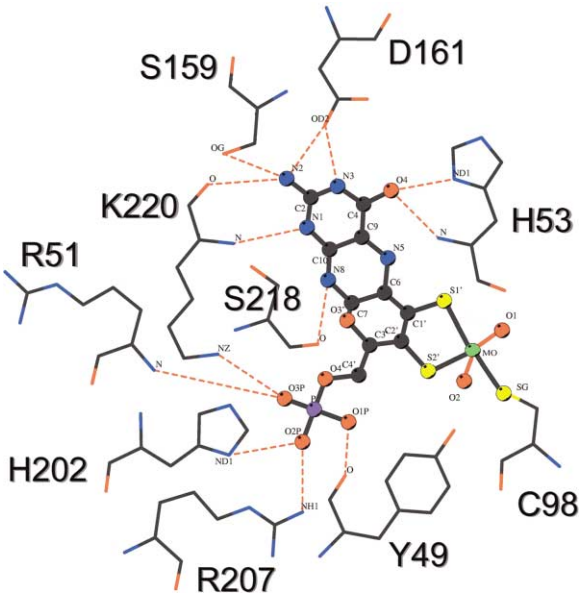

Figure 4. Coordination of the Moco

Schematic representation of the interactions between Moco and PSO. Hydrogen bonds are drawn as red dashed lines. All side chains are conserved between PSO and CSO (compare Figure 2) with the exception of Tyr49 and Ser159. This figure was generated with LIGPLOT (Wallace et al., 1995).

molybdopterin. The presence of a dioxo-Mo center is a common feature of the sulfite oxidase family (Hille, 1996) and, given the limited resolution of this structure, appears to be also present in PSO. In combination with three sulfur atoms, two provided by MPT and one by Cys98 as well as the two oxo ligands, the Mo is coordinated with approximate square pyramidal geometry (Figure 3D). The cofactor is deeply buried in the center of the Moco domain with a funnel leading from the protein surface to the active site (Figure 3A). The Moco is coordinated by 13 direct hydrogen bonds to main chain and side chain atoms of the protein (Figure 4) and no water-mediated hydrogen bonds to the cofactor are observed. The pterin interacts with the protein by eight direct hydrogen bonds involving His53 (N-O4, Nδ1-O4), Ser159 (Oγ-N2), Asp161 (Oδ2-N2, Oδ2-N3), Ser218 (O-N8), and Lys220 (N-N1, O-N2), and the terminal phosphate group is stabilized by five additional hydrogen bonds formed by Tyr49 (O-O1P), Arg51 (N-O3P), His202 (Nδ1-O2P), Arg207 (Nη1-O2P), and Lys220 (Nξ-O3P). In addition, both oxo-ligands of the Mo interact with the protein by four direct hydrogen bonds originating from Arg51 (Nϵ-O2), Ala99 (N-O1), Ala216 (N-O1), and Tyr241 (OH-O2). Almost all residues coordinating the cofactor through side chain hydrogen bonds (Figures 2 and 4) are strictly conserved among SOs and NRs (Eilers et al., 2001; Kisker et al., 1997a). The only exceptions are Tyr49 and Ser159 (Figures 2 and 4), which are unique to plant SO sequences. Ser159 replaces Ala242 of CSO and results in a slightly different cofactor coordination with a new hydrogen bond (Ser159Oγ-N2), allowing the side chain of Asp161 to flip away from the cofactor resulting in a main chain contact with Oδ1. The second oxygen of Asp161 still binds to N2 of the pterin keeping the total number of hydrogen bonds between the Moco and the protein constant in both enzymes.

The longest consensus sequence among the dioxo Mo hydroxylases SO and NR is a 6 amino acid stretch starting with Cys98, which is directly involved in the coordination of the Mo. Cys98 is not part of a secondary structure element, but is flanked by β8 and α3 (Figure 2). This region provides the structural core of the active site in SOs as well as in NRs in which the cysteine is crucial for the activity of these Mo enzymes as shown for human sulfite oxidase by site-directed mutagenesis experiments of Cys185 (Garrett and Rajagopalan, 1996).

The reduced and oxidized form of the Moco have distinct Mo-O bond lengths. PSO was purified under fully oxidizing conditions, and the bond lengths for the two oxo-ligands appeared to be well below 2 Å, suggesting that PSO is in the oxidized Mo(VI) form (George et al., 1989) rather than the reduced Mo(IV) form, in which a water molecule replaces one of the oxo ligands resulting in a Mo-O distance of approximately 2.3 Å (Garton et al., 1997; Kisker et al., 1997a). However, at the present resolution of 2.6 Å, the electron density of ligands is partially obscured by the large electron density peak centered on the Mo center that leads to Fourier ripples (Schindelin et al., 1997) and the Mo-O distances therefore have to be taken with caution.

PSO was initially crystallized in the absence of sulfite or sulfate. After structure determination of the native enzyme, cocrystallization and soaking experiments were performed to bind sulfite or sulfate, but no difference density indicating a bound ligand was observed. This might be due to the crystallization conditions at the relatively high pH of 9.2 leading to deprotonation of some of the positively charged residues in the substrate binding pocket.

Comparison of the Overall Fold of PSO and CSO

The primary sequences of PSO and CSO share 46% identity. Considering the two domains separately, the Moco domains show a slightly higher identity of 48%, whereas 43% of the residues forming the dimerization domains are conserved in both proteins. The longest consecutive consensus sequence between PSO and CSO is represented by 12 identical residues in the Moco domain starting with Val92 (Figure 2). This sequence includes Cys98 that is part of the active site as described earlier. The dimerization domain is less conserved but contains a stretch of 25 amino acids (from Lys287 to Trp311) out of which 18 are highly conserved between the two enzymes.

The homology in primary sequence is reflected by a high structural similarity of both proteins as indicated by an rms deviation of 0.98 Å for 352 out of 388 Cα atoms (Figure 5A). Regions omitted from the superposition were Pro2-Arg8, Leu144-Ala152, Lys164-Gly168, and Glu319-Asp332. The N-terminal residues were excluded from the superposition due to a different conformation of the flexible linker between the cytochrome b_5 and Mo domain in CSO. The second omission covers the insertion of Ser147 to Leu150 in PSO, which form a

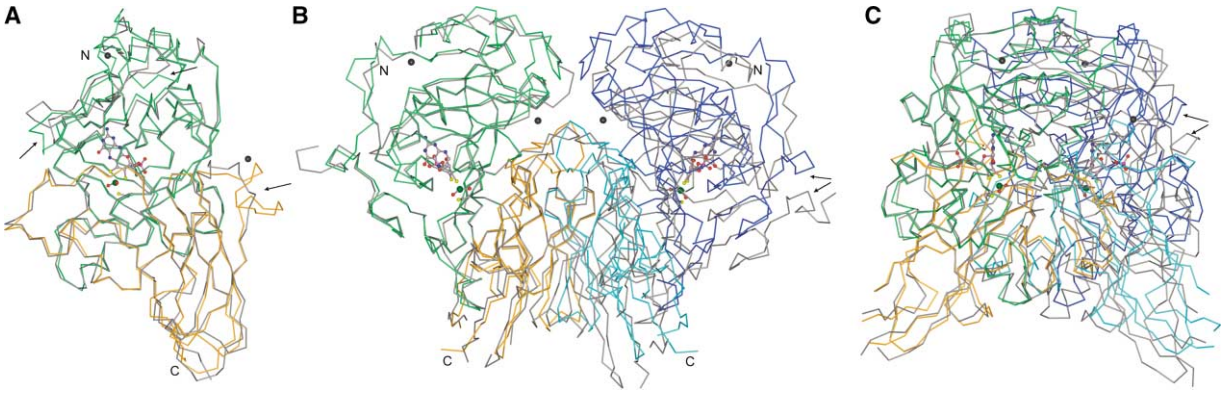

Figure 5. Structural Comparison of PSO and CSO

(A) Superposition of PSO (green and orange) and CSO monomers (gray). The view is the same as in Figure 3A. Structural changes are highlighted by arrows.

(B) Superposition of PSO and CSO dimers. Only one monomer of CSO and PSO was superimposed resulting in the offset between the other monomers (PSO, blue and cyan and CSO, gray). Arrows indicate the rotation of the second monomer.

(C) View of the dimer superposition rotated by 90° compared to (A) along the rotation axis of the monomers.

surface loop between α4 and β10 (Figures 2 and 5). Another insertion (Arg162 and Cys163) might be one reason for conformational changes between β10 and β11 resulting in the formation of an additional helix (3_{10}-2) in PSO. The longest insertion is the extension of a surface loop in PSO by 7 residues (Glu319-Ile325), which alters the structure of the ensuing residues. Comparison of the secondary structure elements of both sulfite oxidases reveals a higher overall number of residues arranged in α helices or β strands for PSO (Figure 2). 130 out of 242 residues of PSO, corresponding to 53.7% of the Moco domain, are part of a secondary structure element compared to 110 amino acids in CSO. The Moco domain of PSO starts with a short β strand (β1), which is lacking in CSO, as well as β5 and helices 3_{10}-1, 3_{10}-2, and 3_{10}-3. The only secondary structure element in CSO that is missing in PSO is α7. The dimerization domains contain an almost equal amount of β strands and α helices formed by 63 out of 151 residues in PSO and 62 out of 148 residues in CSO, respectively. A separate superposition of the individual domains reveals similar rms deviations (0.92 Å for the Moco domain, 0.99 Å for the dimerization domains) as found for the entire monomer, thus demonstrating a conserved orientation of both domains relative to each other. Therefore the PSO and CSO monomers are structurally very similar and PSO adopts the same novel fold as first seen in CSO (Kisker et al., 1997a).

More pronounced differences between both enzymes are observed upon superimposing the dimers, leading to an rms deviation of 1.85 Å for 704 out of 776 residues. The increased deviation by almost a factor of two for the dimers is due to a different orientation of the monomers in the dimer, which is illustrated by the superposition of one monomer of each dimer and the large displacement of the other monomers (Figures 5B and 5C). The second monomer of each dimer is rotated by 10.5 degrees around an axis that is perpendicular to the dimer axis and lies in the plane of the interface, close to Asn361. The change in relative orientation of the subunits within the dimer results in a shorter distance between the Moco domains in the PSO dimer compared to the CSO dimer, but has a smaller effect on the separation of the dimerization domains. For instance, the Leu144 side chains of both subunits of the PSO dimer are in van der Waals distance (with an intersubunit distance of 9.7 Å between Cα atoms of Leu144), while Glu231, the corresponding residue of CSO, is not part of the dimer interface (the corresponding distance between Cα atoms is 17.9 Å). The closer approach of the Moco domains in the PSO dimer is also reflected in a larger number of intersubunit hydrogen bonds, with three side-chain hydrogen bonds in PSO (Ser178, Asn182, Glu184) compared to only one in CSO (between Glu235 and Lys401) (Figure 3E). Neither the three PSO residues nor Glu235 in CSO are conserved. Glu235 in CSO corresponds structurally to Arg153 in PSO that makes a contact to Ser329 in one of the three dimers of the asymmetric unit.

Overall, the plant enzyme contains 20 direct intersubunit hydrogen bonds in contrast to 30 observed in CSO. This finding possibly reflects a weakened dimer as already observed by the detection of monomeric PSO during purification of the recombinantly expressed protein (Figure 1C) (Eilers et al., 2001). For animal SOs only homodimeric enzyme was purified and no evidence was given for a monomeric enzyme. The differences between the PSO and CSO dimers go hand in hand with structural changes in their dimerization domains. One of the most diverging areas is located near the second Cs binding site of PSO (Figure 5A). This includes the loop region between β21 and β22 of PSO with a distance of 9.8 Å between Ser331 of PSO and the corresponding Gly405 of CSO, the maximum deviation in the loop. The average rms deviation for residues Ser326 to Lys333 is 3.2 Å. In PSO, this loop is extended by 7 residues, due to the insertion of Glu319 to Ile325. Consistent with the structural differences, residues located in the loop and in-

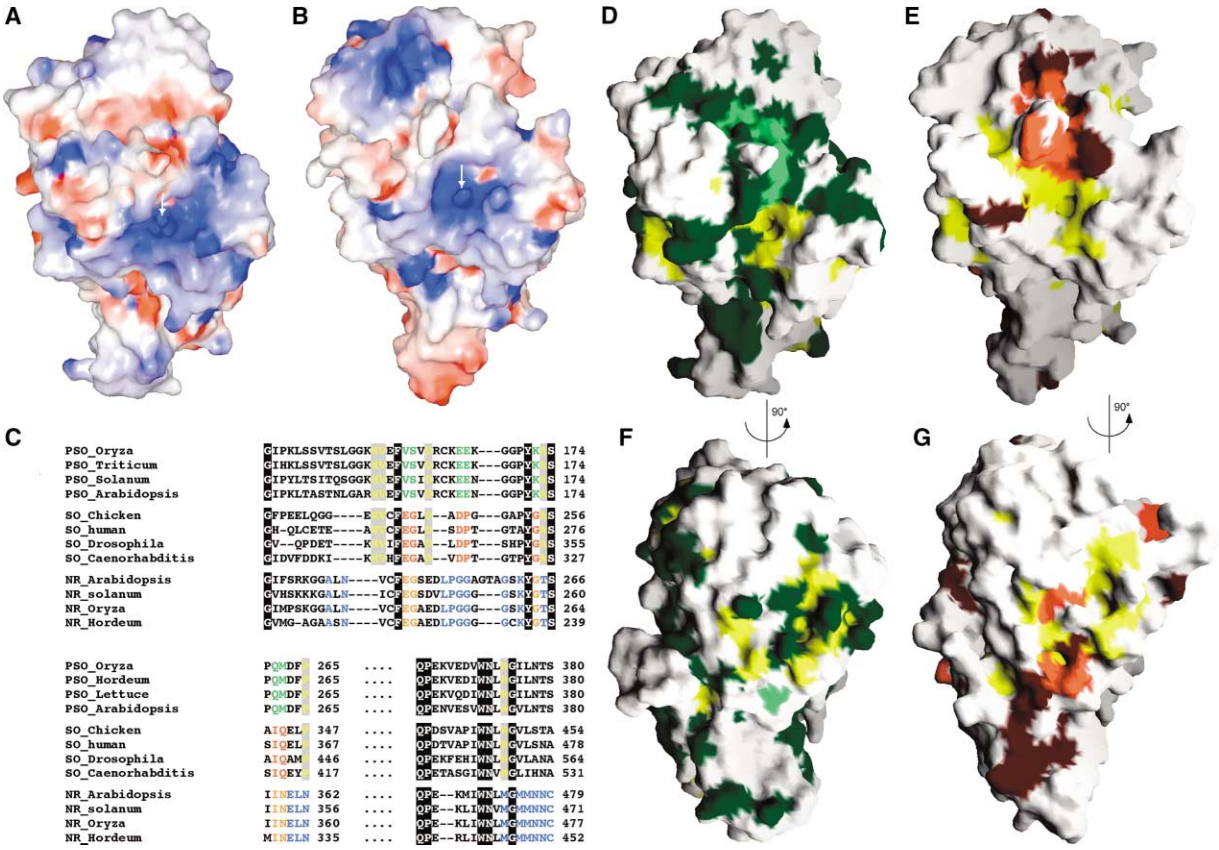

Figure 6. Comparison of PSO and CSO (Mo-Domain) Surfaces

(A and B) Electrostatic surface potentials of PSO (A) and CSO (B). Surface residues are color coded at the same scale according to their charge (blue for positively and red for negatively charged side chains). Hydrophobic areas are not colored. The view is centered on the entrance of the strongly positive charged funnel.

(C) Amino acid sequence alignment of plant (PSO), animal SOs (SO), and nitrate reductases (NR). The sequence alignment was generated with ClustalW (Thompson et al., 1994) and selected areas of conservation are presented (last residue of each block is numbered). The different conservation of residues among the different classes of enzymes is highlighted as follows. Fully conserved residues are shown as white letters with black shadings. Residues, which are only conserved in plant and animal SOs, are shown in yellow with gray shadings. Residues, which are conserved either in PSOs or animal SOs, are shown in bright green (PSO) or bright red (SO). These residues are also highlighted in (D) and (E). Residues exclusively conserved in NR are shown in blue with the exception of those positions that are conserved also in animal SOs (orange).

(D–G) Surface representation of PSO (D and F) and CSO (E and G) with surface residues color coded according to their strict (bright red and green) and individual (dark red and green) conservation in CSO (red) and PSO (green). Residues, which are strictly conserved in all SOs, are highlighted in yellow. Surfaces are viewed into the active site (D and E) and after rotation by 90° (F and G). Surfaces were generated using GRASP (Nicholls et al., 1991) and rendered either with POVRAY (http://www.povray.org) (A and B) or RASTER3D (Merritt and Murphy, 1994) (D–G).

volved in the second Cs binding site show high conservation in all plant sequences known so far, but are not conserved in animals (data not shown). Therefore, this cation binding site might be of structural and functional importance in PSOs.

Surface Properties of PSO and CSO

As shown before, the overall structures of plant and animal SO are very similar, with changes dispersed throughout both domains and, particularly, in the arrangement of the monomers within the dimers. The calculation of an electrostatic surface potential map of both enzymes reveals additional differences in the charge distribution (Figures 6A and 6B). Common to both proteins is a positively charged funnel leading from the surface to the Mo at the active site (see below). Around this funnel, PSO shows a more pronounced positive charge distribution in a wide area stretched almost across the entire width of the protein (Figure 6B). These differences could be a consequence of a different electron acceptor of the plant enzyme.

In the CSO structure, the cytochrome b_5 domain is located far away from the active site yielding a distance between the Mo and Fe atoms of around 32 Å (Kisker et al., 1997a). Internal electron transfer rates for CSO were measured to be 1400 s^{-1} (Pacheco et al., 1999). However, on the basis of current models for internal electron transfer the rate constant should be below 100

s^{-1} for the distance observed in the CSO structure (Page et al., 1999). Furthermore, the observation that an increase in solvent viscosity results in a dramatic reduction of the internal electron transfer rate in CSO gave strong evidence for a movement of the cytochrome b_5 domain (Feng et al., 2002). These results imply major conformational changes in CSO during the catalytic cycle that would bring both cofactors into close spatial proximity. This hypothesis is supported by the fact that both domains are connected via a flexible linker region. One can argue that during catalysis two distinct conformations of CSO exist, one for efficient internal electron transfer to pass electrons derived from sulfite oxidation to the heme, and one for the subsequent oxidation of the heme by cytochrome *c*. In the electron transfer competent state the cytochrome b_5 domain is predicted to efficiently interact through its negatively charged exposed edge with the positively charged substrate entrance of the Moco domain (Kisker et al., 1997a). The high mobility of the cytochrome b_5 domains in CSO is also illustrated by the fact that they adopt slightly different orientations within the CSO dimer.

In plants, the situation is completely different, because *Arabidopsis* SO as well as all other known plant SO sequences lack a b_5 domain and, up to now, no interaction of another separate heme-containing or any other redox protein with PSO has been identified (R.R.M. et al., unpublished data). For bacterial SO, similar to plants, a single Mo domain has been identified, but this forms a subunit that is posttranslationally assembled into a heterodimeric protein complex with a separately expressed heme-type cytochrome c_{552} subunit leading to the formation of active SO in *Thiobacillus novellus* (Kappler et al., 2000). One major question regarding the function and mechanism of plant SO is the identification of the terminal electron acceptor that would complete the catalytic cycle of sulfite oxidation in plants.

Based on the assumption that the proposed interaction between the Moco domain and the b_5 domain should take place in close proximity to the substrate binding site (Feng et al., 2002), a conservation of residues among animal SOs mediating this interaction should be found. Furthermore, assuming a different electron acceptor for plant SOs, a different subset of conserved surface residues should be present in PSO. We have therefore aligned four different animal SO sequences with two complete and four partial PSO sequences. In the surface representations of PSO (Figures 6D and 6F) and CSO (Figures 6E and 6G), we have highlighted residues that are fully conserved in all SOs (yellow), residues that are strictly conserved either in plant (bright green) or animal (bright red) SO families, but differ between the two families, and residues that are conserved or type-conserved in only one family (dark green and red). Figure 6E clearly shows an extended patch of highly conserved surface residues in animal SOs that are in close proximity to the entrance of the active site. They could therefore be appropriate candidates for binding of the cytochrome b_5 domain during internal electron transfer. Unlike most surface residues, these amino acids are fully conserved among mammals, birds, and insects (Figure 6C), suggesting an important site of interaction. In PSO these residues are also invariant, but of a different type (Figure 6D). In addition, the highly conserved residues are surrounded by conserved or type-conserved residues (Figures 6D and 6E), but the degree of conservation is higher in PSO than in CSO.

The crystal structure of the b_5 domain of CSO (Kisker et al., 1997a) revealed negatively charged surface residues at the proposed site of interaction with the Moco domain. In addition to the two propionate groups, Glu67 is in close proximity to the heme and might interact with those residues that are unique to animal SO (Figures 6D and 6E) and surround the active site of the Moco domain. However, these surface residues are also negatively charged. Considering the high flexibility of the heme domain that was shown to be important for efficient intramolecular electron transfer (Feng et al., 2002), it might be feasible that over the course of evolution the conserved binding site of the Moco domain developed a weak rather than a tight interaction between the b_5 and Moco domain. In this way, once reduced, the b_5 domain could swing back into its remote position allowing the interaction with cytochrome c as the physiological electron acceptor. A tight binding, in contrast, could prevent the enzyme from functioning efficiently, since the reduced b_5 domain would be tied up in a stable conformation at the surface of the Moco domain. After rotating both structures by 90° (Figures 6F and 6G), a second surface patch of conservation can be seen in the CSO structure (Figure 6G), which represents the heme binding site as observed in the crystal structure of CSO (Kisker et al., 1997a).

Based on the comparison of the PSO and CSO structures, residues have been identified that appear to be essential for internal electron transfer in plant as well as animal SOs and underline the existence of a different electron acceptor in plant SOs. This hypothesis is further strengthened by the conservation of five out of seven animal SO-specific surface residues in NRs (Figure 6C), which belong to the same class of Moco enzymes. Like animal SOs, NRs also contain a cytochrome b_5 domain that is essential for internal electron transfer, which is predicted to interact in a similar fashion with the Moco domain.

The Active Site

The surface potential calculation of PSO reveals a highly positively charged funnel leading from the protein surface to the Mo in the center of the Moco domain (Figures 6A and 6B), at the end of which is the substrate binding pocket. In the CSO structure, the funnel is occupied by two sulfate ions; one located in close proximity (5.2 Å) of the Mo atom (Kisker et al., 1997a), the other in the wider part of the funnel. In PSO, the length of the funnel is 13.5 Å as measured by the distance from the Mo to Ala24, the last amino acid of β2, as well as Lys239, the last residue of α6. In CSO the funnel is of the same length, but the width at the entrance is significantly enlarged by 7 Å to 22.8 Å compared to 14.5 Å in PSO, which is due to a different conformation of the surface loop between Ala245 and Ala250. The corresponding residues in PSO (Lys164-Gly169) form helix 3_{10}-2 (compare Figures 2, 3, and 5). Interestingly, in the apo-structure of PSO Glu165 occupies the binding site of the

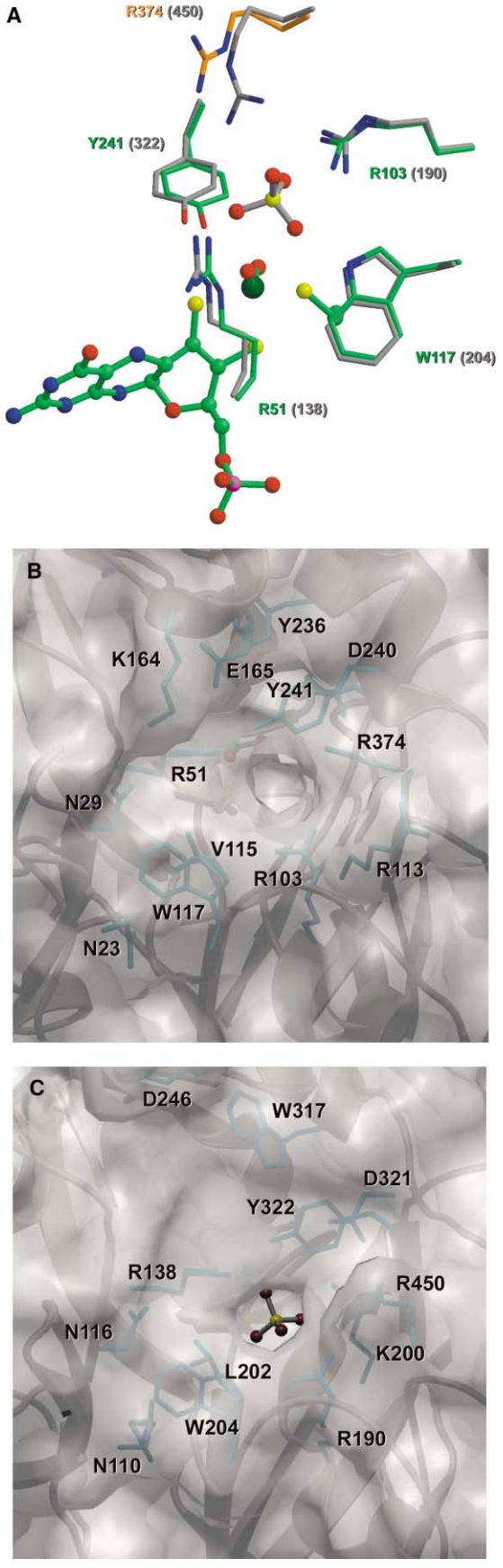

second sulfate molecule found in the CSO structure. Residues 164-169 are well conserved in plant SOs (Figure 6C) as are the corresponding residues in animal SOs (245-250) with the exception of the first residue. These residues might therefore be of importance for the plant-specific electron acceptor.

The crystal structure of CSO provided insights into the substrate/product binding site of SOs due to a bound sulfate derived from the crystallization buffer (Kisker et al., 1997a). The residues responsible for the formation of the binding pocket, Arg138, Arg190, Arg450, Trp204, Tyr322, are all conserved in PSO and except for Arg450 and Tyr322 also in NR (Figure 2). Lys200 of CSO is not directly involved in sulfate binding, but it increases the already mentioned positive charge of the pocket, and is also conserved in NR and type conserved in PSO (Arg113). The conservation of these residues throughout the sulfite oxidase family, including NR, is of particular interest, suggesting a very similar binding pocket for nitrate and nitrite.

The superposition of PSO and CSO active site residues shows a different side chain conformation for Arg374 (Figure 7A). Since all other residues do not show a substantial change, the conformational change of Arg374 is most likely due to the empty substrate binding pocket. As a result of this change, we conclude that this Arg is a crucial residue for substrate binding, since it is rotated away in the PSO structure (open form) and points toward the sulfate in the CSO structure (closed form). Considering that this residue is the only one among the discussed active site residues that is not conserved in NR, we can further argue that Arg374 contributes significantly to the substrate specificity of the anion binding pocket. In all NRs this residue is replaced by methionine, which is reasonable since the substrate nitrate has to be bound with one of the oxygens positioned toward the Mo, so that it can be removed from the nitrogen. Arg374 is located in the C-terminal dimerization domain and could therefore also transmit conformational changes from the active site to the dimer interface.

The observed difference in orientation of the two monomers forming the dimer in PSO compared to CSO (10.5° rotation of the monomers) might be a result of the conformational change of Arg374 in the active site. Arg113, which is in the vicinity of Arg374, adopts a different conformation than the corresponding Lys200 in CSO (Figures 7B and 7C), and Trp250 is also moved toward the dimer interface. A possible conformational change of the dimer as induced by substrate binding has to be proven by structure determination of PSO with substrate and/or product. This might be a reason for the functional

Figure 7. Comparison of PSO and CSO Active Sites

(A) Superposition of the substrate binding sites in PSO and CSO. Residue bonds are color coded in green and orange (PSO) and gray (CSO) according to the color code used in Figure 5. The sulfate found in the CSO crystal structure (gray bonds) and Moco as seen in the PSO structure (green bonds) is shown in ball-and-stick representation.

(B and C) Surface representation of the funnel of PSO (B) and CSO (C) leading to the active site with important residues indicated. (B) and (C) were generated as described for Figures 6D–6G.

importance of dimerization of eukaryotic Moco enzymes. Another important piece of evidence for the crucial role of Arg374 in PSO is the identification of a human patient with a mutation in Gly473 suffering from SO deficiency (Kisker et al., 1997a). Gly473 corresponds to Gly373 in PSO that adopts torsion angles that are normally observed in left-handed helices. Due to its conservation in all SOs it might also be an important structural feature for the proper positioning of Arg374. Besides Arg374, two other residues, Trp117 and Tyr241, move closer to each other in the substrate-free PSO structure. The observed close proximity of Tyr322 in the CSO structure (Tyr241 in PSO) to the Mo center (Kisker et al., 1997a) led to a proposed role of this residue in catalysis and intramolecular electron transfer (Pacheco et al., 1999). Indeed, recent studies using human SO showed greatly reduced intramolecular transfer rates in the corresponding Tyr343Phe mutant (Feng et al., 2003).

The study presented here not only provides a framework for analyzing structure-function relationships of plant SOs, but also a basis to further investigate the mechanism of internal electron transfer in animal SOs. Finally, given the high level of sequence conservation among the Mo domains of PSO, CSO, and NR, both structures suggest a similar fold for the Mo domain of NR but indicate differences in its substrate binding site.

Experimental Procedures

Expression and Purification of PSO

For recombinant expression of PSO as His_6-tagged protein, the previously described pQE80-At-sox plasmid (Eilers et al., 2001) was used. The protein was expressed in the *Escherichia coli* strain TP1000 (Temple et al., 2000) and grown in 2× YT enriched LB medium containing 1 mM Na_2MoO_4. Cells were grown aerobically at 30°C and induced with 0.1 mM isopropyl-β-thiogalactoside at a cell density of A_{600} = 0.08. After 20–24 hr expression, cells were harvested, extracted in lysis buffer (50 mM Tris/HCl, 300 mM NaCl, 10% (v/v) glycerol, and 20 mM imidazole [pH 8.0]), passed twice through a French Press cell, and separated from the lysate by centrifugation at 22,000 *g* for 30 min. This and all subsequent purification steps were performed at 4°C. The supernatant containing PSO was purified on a Ni-NTA superflow matrix (Qiagen). PSO containing fractions were collected, and buffer was exchanged to 20 mM Tris/HCl and 50 mM NaCl (pH 8.0) using PD10 size exclusion columns (Amersham-Pharmacia). PSO was further purified by anion exchange chromatography on a 10 ml SourceQ15 column (Amersham-Pharmacia). Moco-containing PSO did not bind to the column, whereas the inactive Moco-free form of PSO bound to the column and eluted between 250 and 300 mM NaCl. All subsequent work was performed with the active, Moco-containing enzyme. After concentrating the protein, PSO was applied to a preparative 26/60 Superdex 200 size exclusion chromatography column (Amersham-Pharmacia) equilibrated with crystallization buffer (10 mM Tris/HCl and 250 mM NaCl [pH 8.0]). Two peaks containing PSO were obtained that correspond to monomeric and dimeric forms of the enzyme as analyzed by dynamic light scattering. Fractions containing dimeric PSO were collected, pooled, concentrated to 30–60 mg/ml, and stored at –80°C in 20 μl aliquots after flash freezing in liquid nitrogen.

Crystallization and Structure Determination

Initial PSO crystals were obtained at 18°C by vapor diffusion against a reservoir of a 1:1 diluted solution from the Hampton Crystal Screen II (Hampton Research). Protein concentrations used for crystal setups varied from 15 to 60 mg/ml among the different protein batches. Two different crystal forms with hexagonal morphology were obtained, but only one crystallized in a hexagonal space group: P6 with a = b = 212.5 Å, c = 259.1 Å. These crystals diffracted X-rays poorly to only 6.5 Å. The second crystal form belonged to the orthorhombic space group C222 with a = 221.5 Å, b = 346.5 Å and c = 156.7 Å. Optimized crystallization conditions for this form (5%–12% Jeffamine 600, 50 mM Tris/HCl, and 10 mM CsCl [pH 9.2]) resulted in crystals that grew to a final size of 0.4 × 0.2 × 0.2 mm^3 within 4 to 5 days. These crystals diffracted X-rays to 2.4 Å resolution utilizing synchrotron radiation. All subsequent work was performed with the orthorhombic crystal form. Crystals were transferred stepwise into solutions of increasing cryo-protectant concentrations up to a final concentration of 25% glycerol. After equilibration crystals were flash cooled in liquid nitrogen.

Based on the unit cell dimensions and the self-rotation function (data not shown), the crystals were predicted to contain six PSO dimers per asymmetric unit, resulting in a Matthew's coefficient of 2.85 $Å^3$/Da and a solvent content of 57%, respectively. Datasets were collected on beamline X25 at the National Synchroton Light Source, Brookhaven National Laboratories (ADSC Quantum 315 area detector, at a wavelength of 1.1 Å), and on beamline 14-BMC at the Advanced Photon Source, Argonne National Laboratories (ADSC Quantum 4 area detector and a wavelength of 0.9 Å). All datasets were indexed and scaled using DENZO and SCALEPACK (Otwinowski and Minor, 1997). Initial phasing attempts by molecular replacement with the coordinates of the CSO dimer (Kisker et al., 1997a) including the molybdenum cofactor as search model with AMORE (Navaza, 1994) and COMO (Tong, 1996) were unsuccessful. However, the structure was solved with the same search model using the programs MOLREP and BEAST (Bailey, 1994). Initially the positions of two dimers were identified by both programs and a third dimer was fitted manually using the highest electron density peaks corresponding to the positions of the Mo and cesium (Cs) atoms using the program O (Jones et al., 1991). Side chains were replaced with those from PSO using Swiss PDB viewer (Thompson et al., 1994) and fitted manually into the electron density maps. At this point it became clear that the crystals had an unusually high solvent content of 78% (V_M = 5.7 $Å^3$/Da) and only contained three dimers. Six-fold noncrystallographic symmetry (NCS) restraints were maintained throughout the entire refinement process in REFMAC (Murshudov et al., 1997). The weight of the NCS restraints was chosen to minimize R_{free}.

Acknowledgments

We gratefully acknowledge technical assistance by Tanja Otte (TU Braunschweig) and Liqun Wang (SUNY Stony Brook). N.S. was supported by a fellowship from the Deutsche Akademische Austauschdienst (D/00/05497). We also thank the Deutsche Forschungsgemeinschaft (Schw759/3-1 to G.S.) and the National Institutes of Health (GM58198 to C.K.) for financial support. Technical support by the staff at beamlines X25 and X26C at NSLS of Brookhaven National Laboratories, NY, and beamline 14BMC at Argonne National Laboratories, IL, is acknowledged. The NSLS is supported by DOE and the National Institutes of Health, and beamline X26C is supported, in part, by the State University of New York at Stony Brook and its Research Foundation.

Received: April 22, 2003
Revised: June 10, 2003
Accepted: June 10, 2003
Published: September 30, 2003

References

Astashkin, A.V., Raitsimring, A.M., Feng, C., Johnson, J.L., Rajagopalan, K.V., and Enemark, J.H. (2002). Pulsed EPR studies of nonexchangeable protons near the Mo(V) center of sulfite oxidase: direct detection of the alpha-proton of the coordinated cysteinyl residue and structural implications for the active site. J. Am. Chem. Soc. *124*, 6109–6118.

Bailey, S. (1994). The CCP4 suite—programs for protein crystallography. Acta Crystallogr. *D50*, 760–763.

Barton, G.J. (1993). ALSCRIPT: a tool to format multiple sequence alignments. Protein Eng. *6*, 37–40.

Brody, M.S., and Hille, R. (1999). The kinetic behavior of chicken liver sulfite oxidase. Biochemistry *38*, 6668–6677.

Codd, R., Astashkin, A.V., Pacheco, A., Raitsimring, A.M., and Enemark, J.H. (2002). Pulsed ELDOR spectroscopy of the Mo(V)/Fe(III) state of sulfite oxidase prepared by one-electron reduction with Ti(III) citrate. J. Biol. Inorg. Chem. *7*, 338–350.

Cohen, H.J., Betcher-Lange, S., Kessler, D.L., and Rajagopalan, K.V. (1972). Hepatic sulfite oxidase. Congruency in mitochondria of prosthetic groups and activity. J. Biol. Chem. *247*, 7759–7766.

Dias, J.M., Than, M.E., Humm, A., Huber, R., Bourenkov, G.P., Bartunik, H.D., Bursakov, S., Calvete, J., Caldeira, J., Carneiro, C., et al. (1999). Crystal structure of the first dissimilatory nitrate reductase at 1.9 A solved by MAD methods. Struct. Fold. Des. *7*, 65–79.

Dobbek, H., Gremer, L., Meyer, O., and Huber, R. (1999). Crystal structure and mechanism of CO dehydrogenase, a molybdo iron-sulfur flavoprotein containing S-selanylcysteine. Proc. Natl. Acad. Sci. USA *96*, 8884–8889.

Eilers, T., Schwarz, G., Brinkmann, H., Witt, C., Richter, T., Nieder, J., Koch, B., Hille, R., Hansch, R., and Mendel, R.R. (2001). Identification and biochemical characterization of Arabidopsis thaliana sulfite oxidase. A new player in plant sulfur metabolism. J. Biol. Chem. *276*, 46989–46994.

Enroth, C., Eger, B.T., Okamato, K., Nishino, T., Nishino, T., and Pai, E.F. (2000). Crystal structures of bovine milk xanthine dehydrogenase and xanthine oxidase: structure-based mechanism of conversion. Proc. Natl. Acad. Sci. USA *97*, 10723–10728.

Feng, C., Kedia, R.V., Hazzard, J.T., Hurley, J.K., Tollin, G., and Enemark, J.H. (2002). Effect of solution viscosity on intramolecular electron transfer in sulfite oxidase. Biochemistry *41*, 5816–5821.

Feng, C., Wilson, H.L., Hurley, J.K., Hazzard, J.T., Tollin, G., Rajagopalan, K.V., and Enemark, J.H. (2003). Role of conserved tyrosine 343 in intramolecular electron transfer in human sulfite oxidase. J. Biol. Chem. *278*, 2913–2920.

Garrett, R.M., and Rajagopalan, K.V. (1996). Site-directed mutagenesis of recombinant sulfite oxidase: identification of cysteine 207 as a ligand of molybdenum. J. Biol. Chem. *271*, 7387–7391.

Garton, S.D., Garrett, R.M., Rajagopalan, K.V., and Johnson, M.K. (1997). Resonance raman characterization of the molybdenum center in sulfite oxidase—identification of Mo=O stretching modes. J. Am. Chem. Soc. *119*, 2590–2591.

George, G.N., Kipke, C.A., Prince, R.C., Sunde, R.A., Enemark, J.H., and Cramer, S.P. (1989). Structure of the active site of sulfite oxidase. X-ray absorption spectroscopy of the Mo(IV), Mo(V), and Mo(VI) oxidation states. Biochemistry *28*, 5075–5080.

Heber, U., and Hüve, K. (1998). Action of SO_2 on plants and metabolic detoxification of SO_2. Int. Rev. Cytol. *177*, 255–286.

Hille, R. (1996). The mononuclear molybdenum enzymes. Chem. Rev. *96*, 2757–2816.

Hille, R. (2002). Molybdenum enzymes containing the pyranopterin cofactor: an overview. In Molybdenum and Tungsten. Their Roles in Biological Processes, A. Sigel, and H. Sigel, eds. (New York: M. Dekker), pp. 187–226.

Hutchinson, E.G., and Thornton, J.M. (1996). PROMOTIF--a program to identify and analyze structural motifs in proteins. Protein Sci. *5*, 212–220.

Janin, J., Miller, S., and Chothia, C. (1988). Surface, subunit interfaces and interior of oligomeric proteins. J. Mol. Biol. *204*, 155–164.

Johnson, J.L., and Rajagopalan, K.V. (1977). Tryptic cleavage of rat liver sulfite oxidase. Isolation and characterization of molybdenum and heme domains. J. Biol. Chem. *252*, 2017–2025.

Johnson, J.L., and Rajagopalan, K.V. (1979). The oxidation of sulphite in animals systems. Ciba Found. Symp. *72*, 119–133.

Jones, T.A., Zou, J.Y., Cowan, S.W., and Kjeldgaard, M. (1991). Improved methods for building protein models in electron density maps and the location of errors in these models. Acta Crystallogr. *A47*, 110–119.

Kappler, U., Bennett, B., Rethmeier, J., Schwarz, G., Deutzmann, R., McEwan, A.G., and Dahl, C. (2000). Sulfite : Cytochrome c oxidoreductase from *Thiobacillus novellus* - Purification, characterization, and molecular biology of a heterodimeric member of the sulfite oxidase family. J. Biol. Chem. *275*, 13202–13212.

Kisker, C., Schindelin, H., Pacheco, A., Wehbi, W.A., Garrett, R.M., Rajagopalan, K.V., Enemark, J.H., and Rees, D.C. (1997a). Molecular basis of sulfite oxidase deficiency from the structure of sulfite oxidase. Cell *91*, 973–983.

Kisker, C., Schindelin, H., and Rees, D.C. (1997b). Molybdenum-cofactor-containing enzymes: structure and mechanism. Annu. Rev. Biochem. *66*, 233–267.

Kraulis, P.J. (1991). MOLSCRIPT—a program to produce both detailed and schematic plots of protein structures. J. Appl. Crystallogr. *24*, 946–950.

Laskowski, R.A., Moss, D.S., and Thornton, J.M. (1993). Main-chain bond lengths and bond angles in protein structures. J. Mol. Biol. *231*, 1049–1067.

Leustek, T., and Saito, K. (1999). Sulfate transport and assimilation in plants. Plant Physiol. *120*, 637–644.

McMaster, J., and Enemark, J.H. (1998). The active sites of molybdenum- and tungsten-containing enzymes. Curr. Opin. Chem. Biol. *2*, 201–207.

Mendel, R.R., and Schwarz, G. (1999). Molybdoenzymes and molybdenum cofactor in plants. Crit. Rev. Plant Sci. *18*, 33–69.

Merritt, E.A., and Murphy, M.E.P. (1994). Raster3D Version 2.0—a program for photorealistic molecular graphics. Acta Crystallogr. *D50*, 869–873.

Murshudov, G., Vagin, A., and Dodson, E. (1997). Refinement of macromolecular structures by the maximum likelihood method. Acta Crystallogr. *D53*, 240–255.

Navaza, J. (1994). AMORE—an automated package for molecular replacement. Acta Crystallogr. *A50*, 157–163.

Nicholls, A., Sharp, K.A., and Honig, B. (1991). Protein folding and association: Insights from the interfacial and thermodynamic properties of hydrocarbons. Proteins *11*, 281–296.

Otwinowski, Z., and Minor, W. (1997). Processing of X-ray diffraction data collected in oscillation mode. In Methods in Enzymology—Macromolecular Crystallography, C.W. Carter and R.M. Sweet, eds. (Academic Press), pp. 307-326.

Pacheco, A., Hazzard, J.T., Tollin, G., and Enemark, J.H. (1999). The pH dependence of intramolecular electron transfer rates in sulfite oxidase at high and low anion concentrations. J. Biol. Inorg. Chem. *4*, 390–401.

Page, C.C., Moser, C.C., Chen, X., and Dutton, P.L. (1999). Natural engineering principles of electron tunnelling in biological oxidation-reduction. Nature *402*, 47–52.

Raitsimring, A.M., Pacheco, A., and Enemark, J.H. (1998). ESEEM investigations of the high and low pH forms of chicken liver sulfite oxidase. J. Am. Chem. Soc. *120*, 11263–11278.

Rajagopalan, K.V., and Johnson, J.L. (1992). The pterin molybdenum cofactors. J. Biol. Chem. *267*, 10199–10202.

Romao, M.J., Archer, M., Moura, I., Moura, J.J., LeGall, J., Engh, R., Schneider, M., Hof, P., and Huber, R. (1995). Crystal structure of the xanthine oxidase-related aldehyde oxido- reductase from D. gigas. Science *270*, 1170–1176.

Schindelin, H., Kisker, C., Hilton, J., Rajagopalan, K.V., and Rees, D.C. (1996). Crystal structure of DMSO reductase: redox-linked changes in molybdopterin coordination. Science *272*, 1615–1621.

Schindelin, H., Kisker, C., and Rees, D.C. (1997). The molybdenum-cofactor: a crystallographic perspective. J. Biol. Inorg. Chem. *2*, 773–781.

Shih, V.E., Abroms, I.F., Johnson, J.L., Carney, M., Mandell, R., Robb, R.M., Cloherty, J.P., and Rajagopalan, K.V. (1977). Sulfite oxidase deficiency. Biochemical and clinical investigations of a hereditary metabolic disorder in sulfur metabolism. N. Engl. J. Med. *297*, 1022–1028.

Temple, C.A., Graf, T.N., and Rajagopalan, K.V. (2000). Optimization of expression of human sulfite oxidase and its molybdenum domain. Arch. Biochem. Biophys. *383*, 281–287.

Thompson, J.D., Higgins, D.G., and Gibson, T.J. (1994). CLUSTAL W: improving the sensitivity of progressive multiple sequence alignment through sequence weighting, position-specific gap penalties and weight matrix choice. Nucleic Acids Res. *22*, 4673–4680.

Tong, L. (1996). Combined molecular replacement. Acta Crystallogr. *A52*, 782–784.

Truglio, J.J., Theis, K., Leimkuhler, S., Rappa, R., Rajagopalan, K.V., and Kisker, C. (2002). Crystal Structures of the Active and Alloxanthine-Inhibited Forms of Xanthine Dehydrogenase from Rhodobacter capsulatus. Structure (Camb) *10*, 115–125.

Wallace, A.C., Laskowski, R.A., and Thornton, J.M. (1995). LIGPLOT: A program to generate schematic diagrams of protein-ligand interactions. Prot Eng *8*, 127–134.

Accession Numbers

Atomic coordinates of *Arabidopsis* sulfite oxidase were deposited in the RCSB Protein Data Bank with PDB entry 1OGP.